

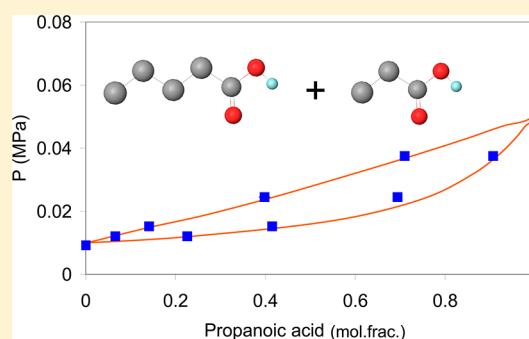
Prediction of Phase Equilibrium and Hydration Free Energy of Carboxylic Acids by Monte Carlo Simulations

Nicolas Ferrando,* Ibrahim Gedik, Véronique Lachet, Laurent Pigeon, and Rafael Lugo

IFP Energies Nouvelles, 1 et 4 avenue de Bois-Préau, 92852 Rueil-Malmaison, France

S Supporting Information

ABSTRACT: In this work, a new transferable united-atom force field has been developed to predict phase equilibrium and hydration free energy of carboxylic acids. To take advantage of the transferability of the AUA4 force field, all Lennard-Jones parameters of groups involved in the carboxylic acid chemical function are reused from previous parametrizations of this force field. Only a unique set of partial electrostatic charges is proposed to reproduce the experimental gas phase dipole moment, saturated liquid densities and vapor pressures. Phase equilibrium properties of various pure carboxylic acids (acetic acid, propanoic acid, butanoic acid, pentanoic acid, hexanoic acid) and one diacid (1,5-pentanedioic) are studied through Monte Carlo simulations in the Gibbs ensemble. A good accuracy is obtained for pure compound saturated liquid densities and vapor pressures (average deviation of 2% and 6%, respectively), as well as for critical points. The vaporization enthalpy is, however, poorly predicted for short acids, probably due to a limitation of the force field to correctly describe the significant dimerization in the vapor phase. Pressure–composition diagrams for two binary mixtures (acetic acid + *n*-butane and propanoic acid + pentanoic acid) are also computed with a good accuracy, showing the transferability of the proposed force field to mixtures. Hydration free energies are calculated for three carboxylic acids using thermodynamic integration. A systematic overestimation of around 10 kJ/mol is observed compared to experimental data. This new force field parametrized only on saturated equilibrium properties appears insufficient to reach an acceptable precision for this property, and only relative hydration free energies between two carboxylic acids can be correctly predicted. This highlights the limitation of the transferability feature of force fields to properties not included in the parametrization database.



1. INTRODUCTION

The knowledge of thermophysical properties and phase equilibrium of systems involving carboxylic acids is of great interest in many industrial applications, e.g., biochemistry, pharmaceuticals, oil, and gas industries. The industrial processes of biomass valorization to produce biofuels or biochemical products often involve large amounts of carboxylic acids that have to be separated from the final product. The acid content of a typical bio-oil produced from biomass pyrolysis can for example reach up to 25 wt %.^{1,2} Free-fatty carboxylic acids are also present in vegetable oil blends and have to be converted to increase biodiesel production yield.^{3,4} The separation units often involve distillation columns and liquid–liquid extractors, and their design thus requires a good knowledge of both liquid–vapor phase equilibrium and partition coefficient of acids between two liquid solvents, which can be calculated from solvation free energy. Due to the large variety of acids and properties to be studied, the use of predictive models is necessary to reduce the number of experiments to carry out. We propose in this work to use molecular simulation with a new transferable force field to predict these properties.

Molecular simulation is becoming an efficient tool to predict thermodynamic data and phase equilibrium of pure compounds and mixtures for industrial applications. Transferable united

atom force fields are currently developed to simulate a large number of molecules and properties with an acceptable precision and a reduced computational time.^{5–7} Briggs et al. have proposed a first united atom force field for carboxylic acids as an extension of the OPLS-UA force field by reusing existing groups and proposing a specific electrostatic charge distribution.⁸ This model is, however, limited to acetic acid at moderate temperatures, and saturated properties significantly deviate from experiments at high temperature.⁹ This force field can not be consequently considered as transferable. An extension of the TraPPE-UA force field¹⁰ to acids was proposed by Kamath et al.⁹ by introducing a new group for the carboxyl carbon atom and by using a unique set of electrostatic charges determined from an *ab initio* calculation. This model accurately predicts saturated liquid densities and critical properties of short and long alkyl-chain acids, but significantly overestimates vapor pressures (deviations up to 40%). Clifford et al. used this force field to predict phase equilibrium of binary mixtures, but overestimation of pure compound vapor pressures naturally leads to overestimate bubble pressures of the mixture whatever

Received: February 4, 2013

Revised: April 17, 2013

Published: May 22, 2013



the composition.¹¹ Finally, this state of the art shows that some improvements can be brought in the domain of united atom force fields to be more accurate on a larger number of equilibrium properties. Thus, we propose in this work an extension of the transferable AUA4 force field to carboxylic acids. This force field has been specially developed to predict phase equilibrium of pure compounds and mixtures involving linear alkanes,¹² branched and cyclic alkanes,^{13,14} olefins,¹⁵ benzene,^{16,17} alkyl-benzene,^{18,19} polyaromatic hydrocarbons,^{20,21} sulfur compounds,^{22,23} alcohols,²⁴ ketones,²⁵ aldehydes,²⁵ ethers,²⁶ esters,²⁷ and amines.^{28,29} To highlight the transferability of the new force field proposed, short and long alkyl-chain carboxylic acids (from acetic acid to hexanoic acid) and a diacid (1,5-pentanedioic acid) are studied. Pure compounds and binary mixtures are considered. Saturated properties, critical properties, and liquid phase structure are investigated through Monte Carlo simulations, as well as hydration free energy of various acids using thermodynamic integration.

This paper is organized as follows: the new force field is described in section 2. The simulation methods to calculate bulk properties and hydration free energy are detailed in section 3. Section 4 deals with simulation results, and section 5 provides our conclusions.

2. FORCE FIELD

2.1. Intermolecular Energy. The dispersive-repulsive intermolecular interactions between two force centers i and j are described through a 12–6 Lennard-Jones (LJ) potential:

$$U_{ij}^{\text{LJ}} = 4\epsilon_{ij} \left[\left(\frac{\sigma_{ij}}{r_{ij}} \right)^{12} - \left(\frac{\sigma_{ij}}{r_{ij}} \right)^6 \right] \quad (1)$$

where r_{ij} , ϵ_{ij} , σ_{ij} are the distance, the LJ well depth, and the LJ size, respectively.

The Lorentz–Berthelot combining rules are used to obtain the cross LJ parameters:

$$\epsilon_{ij} = \sqrt{\epsilon_{ii}\epsilon_{jj}} \quad (2)$$

$$\sigma_{ij} = \frac{1}{2}(\sigma_{ii} + \sigma_{jj}) \quad (3)$$

The carboxylic acids studied in this work involve five different groups: CH_3 , CH_2 , $\text{C}(=)$, $(=)\text{O}$, and OH . To take advantage of the transferability of the AUA4 force field, all the Lennard-Jones parameters are reused from previous parametrizations: alkanes for the CH_x groups,¹² ketones for the $\text{C}(=)$ and $(=)\text{O}$ groups,²⁵ and alcohols for the OH group²⁴ (see illustration in Figure S.1 in the Supporting Information). Thus, no additional parameter has to be introduced. In the AUA model, the Lennard-Jones center is not located on the atomic nucleus of the group, but slightly shifted by a distance δ (AUA displacement) in order to implicitly take into account the presence of its bonded hydrogen atoms. This parameter is also directly transferred from these previous parametrizations.

The electrostatic interaction between two partial electrostatic charges i and j is modeled by the Coulomb potential:

$$U_{ij}^{\text{elec}} = \frac{q_i q_j}{4\pi\epsilon_0 r_{ij}} \quad (4)$$

where r_{ij} is the distance between charges i and j , q_i the magnitude of charge i and ϵ_0 the vacuum permittivity. As for

previous united atoms force fields for acids (OPLS-UA⁸ and TraPPE-UA⁹), we adopt a distribution of five electrostatic charges, one located on the CH_x group next to the acid function, one on the carboxyl carbon, one on the carboxyl oxygen atom, one on the hydroxyl oxygen atom, and one on the hydroxyl hydrogen atom. The use of a unique set of electrostatic charges for all the acids studied here is justified as long as the molecules have a similar dipole moment. As shown in Figure S.2 in the Supporting Information, the experimental gas phase dipole moment³⁰ of linear acids does not significantly vary with the alkyl chain length: the deviation between acetic acid and hexanoic acid dipole moments is less than 8%, and we assume this deviation to be sufficiently low for us to be able to directly transfer the electrostatic charges from one acid molecule to another. The magnitude of the electrostatic charges q_i is determined to obtain the gas phase dipole moment of acetic acid (1.7 D) in its most stable conformation and using the AUA4 bond lengths and angles (Table 2):

$$\left\| \sum_{i=1}^5 q_i \mathbf{r}_i \right\| = \mu_{\text{acetic acid}} \quad (5)$$

where \mathbf{r}_i is the i th charge position given by the intramolecular parameters of the AUA4 force field. As a five charge distribution is adopted, the solution of eq 5 is not unique. Thus, with a constraint to keep the dipole moment equal to 1.7 D, charges are tuned to obtain better predictions of saturated liquid densities and vapor pressures of both acetic and butanoic acids. The resulting electrostatic charges are reported in Table 1.

Table 1. Non-Bonded Parameters for Groups Involved in the Molecules Studied

group	ϵ (K)	σ (Å)	δ (Å)	q (e)
$\text{CH}_3(-\text{CH}_x)$	120.15	3.607	0.216	0
$\text{CH}_3(-\text{C}_{\text{acid}})$	120.15	3.607	0.216	−0.120
$\text{CH}_2(-\text{CH}_x)$	86.29	3.461	0.384	0
$\text{CH}_2(-\text{C}_{\text{acid}})$	86.29	3.461	0.384	−0.120
$\text{C}(=\text{O})$	61.90	3.020	0	+0.658
$\text{O}(=\text{C})$	96.51	2.981	0	−0.506
$\text{O}(-\text{H})$	125.01	3.081	0.01	−0.437
$\text{H}(-\text{O})$	0	0	0	+0.405

2.2. Intramolecular energy. All the bonded parameters involved in the intramolecular energy calculation are given in Table 2. In the proposed force field, all bond lengths are kept fixed and are taken from the alcohol and carboxylate ester AUA4 parametrizations.^{24,27} Atoms separated by two bonds interact via a harmonic bending potential:

$$\frac{U_{\text{bend}}}{k_{\text{B}}} = \frac{1}{2} k_{\text{bend}} (\cos \theta - \cos \theta_0)^2 \quad (6)$$

where k_{B} is the Boltzmann constant, k_{bend} is the bending constant, and θ and θ_0 are the bending angle and the equilibrium bending angle, respectively. Again, all bending constants and equilibrium angles are taken from alcohol and carboxylate ester AUA4 parametrizations, assuming that parameters of the $(=)\text{C}-\text{O}-\text{H}$ angle are identical to those of the $\text{CH}_x-\text{O}-\text{H}$ angle. For atoms separated by three bonds, a torsion potential of the following form is used:

Table 2. Bonded Parameters for Groups Involved in the Studied Molecules

bond length		r_0 (Å)
CH_x-CH_y		1.535
$\text{CH}_x-\text{C}(=\text{O})$		1.522
$\text{C}(=\text{O})=\text{O}$		1.229
$\text{C}(\text{OH})-\text{O}$		1.425
$\text{O}-\text{H}$		0.945
bend	θ_0 (deg)	k_{bend} (K)
$\text{CH}_x-\text{CH}_2-\text{CH}_y$	114.0	74900
$\text{CH}_x-\text{CH}_2-\text{C}(=\text{O})$	114.0	74900
$\text{CH}_x-\text{C}(=\text{O})=\text{O}$	120.4	105822
$\text{CH}_x-\text{C}(=\text{O})-\text{OH}$	119.2	105822
$\text{O}(=\text{C})=\text{C}-\text{OH}$	120.4	105822
$\text{C}(=\text{O})-\text{O}-\text{H}$	108.5	61000
torsion		a_i (K)
$\text{CH}_x-\text{CH}_2-\text{CH}_2-\text{CH}_y$	$a_0 = 1001.35$	$a_1 = 2129.52$
	$a_2 = -303.06$	$a_3 = -3612.27$
	$a_4 = 2226.71$	$a_5 = 1965.93$
	$a_6 = -4489.34$	$a_7 = -1736.22$
$\text{CH}_x-\text{CH}_2-\text{CH}_2-\text{C}(=\text{O})$	$a_8 = 2817.37$	
	$a_0 = 2192.4$	$a_1 = 630.0$
	$a_2 = -1562.4$	$a_3 = 0$
	$a_4 = 0$	$a_5 = 0$
$\text{CH}_x-\text{CH}_2-\text{C}(=\text{O})=\text{O}$	$a_6 = 0$	$a_7 = 0$
	$a_8 = 0$	
	$a_0 = 2192.4$	$a_1 = -630.0$
	$a_2 = -1562.4$	$a_3 = 0$
$\text{CH}_x-\text{CH}_2-\text{C}(=\text{O})-\text{OH}$	$a_{4-8} = 0$	
	$a_0 = 2192.4$	$a_1 = 630$
	$a_2 = -1562.4$	$a_3 = 0$
	$a_{4-8} = 0$	
$\text{H}-\text{O}-\text{C}(=\text{O})=\text{O}$	$a_0 = 2192.4$	$a_1 = -630$
	$a_2 = -1562.4$	$a_3 = 0$
	$a_{4-8} = 0$	
	$a_0 = 2192.4$	$a_1 = -630$
$\text{H}-\text{O}-\text{C}(=\text{O})-\text{CH}_x$	$a_2 = -1562.4$	$a_3 = 0$
	$a_{4-8} = 0$	
	$a_0 = 2192.4$	$a_1 = -630$
	$a_2 = -1562.4$	$a_3 = 0$

$$\frac{U_{\text{tors}}}{k_B} = \sum_{n=0}^8 a_n (\cos(\varphi + \pi))^n \quad (7)$$

where φ is the dihedral angle, and a_i the i th torsion parameter. The $\text{CH}_x-\text{CH}_2-\text{C}=\text{O}$, $\text{CH}_x-\text{CH}_2-\text{C}(=\text{O})-\text{O}$, $\text{CH}_x-\text{C}(=\text{O})-\text{O}-\text{H}$ and $\text{O}=\text{C}-\text{O}-\text{H}$ torsions are taken from the TraPPE-UA force field as proposed by Clifford et al.¹¹ All the other torsions are taken from AUA4 force field.

Finally, a 12-6 Lennard-Jones potential is used to calculate the repulsive-dispersive intramolecular energy between two force centers separated by more than three bonds with identical parameters to those used for intermolecular interactions. Intramolecular electrostatic energy is also taken into account to simulate the diacid studied in this work (1,5-pentanedioic). Coulombic interactions are computed between charges related to atoms separated by more than three bonds.

3. SIMULATION METHODS

3.1. Phase Equilibrium. All the bulk liquid/vapor equilibrium simulations of pure compounds were carried out in the NVT Gibbs Ensemble.^{31,32} In this ensemble, the two phases in equilibrium are introduced in two separate boxes without an explicit interface. When employed to study pure component equilibrium, this ensemble is applied at constant total volume of the two phases in order to respect the phase

rule, the temperature, and the total number of molecules being also imposed. A total number of 300 to 600 molecules was used for each system according to the vicinity of the critical point. The average properties are computed during a production run lasting for 20 million Monte Carlo steps, one step corresponding to a single Monte Carlo move. Before each production run, a preliminary run lasting for 50 to 100 million Monte Carlo steps is carried out to achieve equilibrium. In the case of Lennard-Jones interactions, a spherical cutoff equal to half of the simulation box was used while the classical tail correction was employed.³³ For long-range electrostatic energy, the Ewald summation technique was used, with a number of reciprocal vectors k equal to 7 in all three space directions and a Gaussian width α^{red} equal to 1.8 in reduced units. The different Monte Carlo moves and their corresponding attempt probabilities used during the simulations are molecular translation (20%), molecular rotation (20%), regrowth with configurational bias³⁴ (20%), transfer of a molecule between boxes with preinsertion bias³⁵ (39.5%), and volume change (0.5%). The amplitude of translations, rigid rotations and volume changes was adjusted during the simulation to achieve an acceptance ratio of 40% for these moves. Note that the impact of this last parameter has been checked by resimulating acetic acid at 450K with an acceptance ratio of 50%: the same results were found within statistical uncertainties. The simulations were carried out using the GIBBS software jointly developed by IFP Energies nouvelles and the Laboratoire de Chimie Physique (CNRS-Université Paris-Sud).⁷ The CPU time required for a simulation is typically 48 h using eight cores (2.4 GHz).

The critical properties T_C and ρ_C of pure compounds were estimated by a least-squares fit of the law of rectilinear diameters:

$$\frac{\rho_l + \rho_v}{2} = \rho_C + A(T - T_C) \quad (8)$$

where ρ_l and ρ_v are the density of the liquid and vapor phases respectively, T is the temperature, and A is an adjustable parameter, and the critical scaling relation:

$$\rho_l - \rho_v = B(T - T_C)^\beta \quad (9)$$

where B is another adjustable parameter, and β is the universal exponent, equal to 0.325.³⁴ This procedure has been successfully applied for the prediction of the critical properties of various oxygenated molecules using the AUA4 force field such as alcohols,²⁴ ketones, aldehydes,²⁵ ethers,²⁶ and esters.²⁷ Finally, the normal boiling temperatures of the pure compounds were determined using the Clausius-Clapeyron equation. Note that vapor pressure is calculated using the Virial equation in the vapor phase, and the molar vaporization enthalpy h^{vap} with the following relationship:

$$h^{\text{vap}} = N_A \left(\frac{\langle U^{\text{vap}} \rangle}{\langle N^{\text{vap}} \rangle} - \frac{\langle U^{\text{liq}} \rangle}{\langle N^{\text{liq}} \rangle} + P^{\text{vap}} \left(\frac{\langle V^{\text{vap}} \rangle}{\langle N^{\text{vap}} \rangle} - \frac{\langle V^{\text{liq}} \rangle}{\langle N^{\text{liq}} \rangle} \right) \right) \quad (10)$$

where N_A is the Avogadro number, P^{vap} the pressure calculated in the vapor phase, and $\langle U^i \rangle$, $\langle N^i \rangle$ and $\langle V^i \rangle$ are the average potential energy, total number of molecules, and volume of phase i , respectively.

The simulations of binary mixtures (acetic acid + *n*-butane and propanoic acid + pentanoic acid) are carried out in the NPT Gibbs ensemble.^{32,36} A total number of 700 molecules is

used, and a typical simulation run lasted for 220 million Monte Carlo steps including an equilibrium run of 150 million Monte Carlo steps. Other simulation parameters are identical to those previously described for pure compound simulations. Note that the equilibrium run is longer than for pure compounds probably due to the larger number of molecules used. Indeed, a step is related to a single Monte Carlo move. Thus, a larger number of steps should be carried out to ensure that each molecule is subjected to significant changes in position and conformation.

3.2. Hydration Free Energy. Various molecular modeling methods have been developed to estimate free energies, such as free energy perturbation,³⁷ thermodynamic integration,³⁴ slow-growth method³⁸ or umbrella sampling.³⁹ Many of these methods have been reviewed in specific textbooks.^{40,41} In this work, the thermodynamic integration method will be used in association with Monte Carlo simulations. The use of this method to calculate hydration Gibbs energy of polar and nonpolar solutes has been nicely described elsewhere,^{42–44} and only basics and specific simulation details are given here. The hydration free energy ΔG^{hyd} is defined by the free energy difference given by the total reversible work associated with changing the Hamiltonian of the system from the gas (vacuum) to the liquid phase.⁴⁰ As free energy is a state function, it can be calculated from a thermodynamic cycle including nonphysical

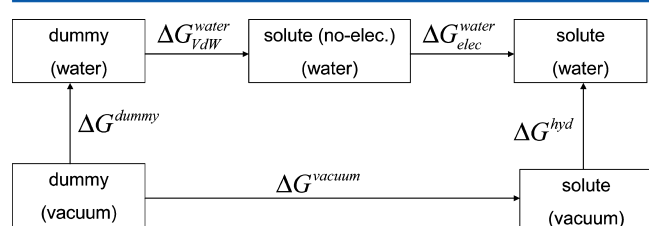


Figure 1. Thermodynamic cycle for hydration free energy calculation.

transformations, as shown in Figure 1. Following this cycle, the hydration free energy is given by

$$\Delta G^{\text{hyd}} = \Delta G^{\text{water}}_{\text{vdW}} + \Delta G^{\text{water}}_{\text{elec}} + \Delta G^{\text{dummy}} - \Delta G^{\text{vacuum}} \quad (11)$$

As discussed by Shirts et al., the terms $\Delta G^{\text{water}}_{\text{vdW}}$ and $\Delta G^{\text{water}}_{\text{elec}}$ correspond to the free energy of “insertion” of the bonded assembly of uncharged Lennard-Jones spheres and to the free energy required for “charging” the solute.⁴⁴ The term ΔG^{vacuum} corresponds to the same transformation, but in vacuum instead of solvent. It is therefore only related to the intramolecular dispersion–repulsion and electrostatic energy. The molecules studied in this work for hydration free energies (acetic acid, propanoic acid, and butanoic acid) do not involve intramolecular electrostatic interaction. Thus, the decomposition between an “insertion” and a “charging” part is not necessary for the ΔG^{vacuum} calculation. Finally, the term ΔG^{dummy} is the solvation free energy of a noninteracting particle (that is, a particle without intermolecular van der Waals or electrostatic interaction energy, but with the same intramolecular energy as the solute), and is equal to zero. The thermodynamic integration method consists in evaluating a free energy difference using the following expression:

$$\Delta G = \int_0^1 \left\langle \frac{\partial U(\lambda)}{\partial \lambda} \right\rangle d\lambda \quad (12)$$

where U is the interaction potential between solute and solvent, and λ is a coupling variable: $\lambda = 1$ means a full coupling between the solute and the solvent molecules, while $\lambda = 0$ means that solute does not interact with the solvent. A fundamental of the thermodynamic integration method is the choice of the coupling function in the interaction potential. The most simple function is probably a linear pathway to go from the initial state A to the final state B:

$$U = (1 - \lambda)U_A + \lambda U_B \quad (13)$$

This formulation could be however problematic since for low λ values, a solute and a solvent molecule could overlap and generate singularities in energy calculation. Beutler et al. proposed a smart solution to overcome this problem by introducing a soft-core potential between solute and solvents for dispersion–repulsion interactions:⁴⁵

$$U_{ij}^{\text{disp-rep}} = 4\epsilon_{ij}\lambda_{\text{vdW}}^n \left[\frac{1}{\left[\alpha(1 - \lambda_{\text{vdW}})^2 + \left(\frac{r_{ij}}{\sigma_{ij}}\right)^6 \right]^2} - \frac{1}{\alpha(1 - \lambda_{\text{vdW}})^2 + \left(\frac{r_{ij}}{\sigma_{ij}}\right)^6} \right] \quad (14)$$

As suggested by Shirts et al., values of 0.5 and 4 are used for α and n , respectively.⁴⁴

The electrostatic energy could be treated by a similar way, but the calculation of long-range corrections becomes not obvious. Practically, many authors use the following coupling function:^{44,46–48}

$$U_{ij}^{\text{elec}} = \frac{\lambda_C q_i q_j}{4\pi\epsilon_0 r_{ij}} \quad (15)$$

As a charge overlap could generate a singularity, the calculation of electrostatic energy for the various values of λ_C should be carried out for $\lambda_{\text{vdW}} = 1$ to ensure sufficient repulsion between atoms bearing electrostatic charges. The complete methodology can be summarized as follows: First, $\Delta G^{\text{water}}_{\text{vdW}}$ is calculated by fixing $\lambda_C = 0$ and by performing one Monte Carlo simulation per value of λ_{vdW} . The following 23 values of λ_{vdW} are selected: {0, 0.05, 0.1, 0.15, 0.2, 0.25, 0.3, 0.35, 0.4, 0.425, 0.45, 0.475, 0.5, 0.55, 0.6, 0.65, 0.7, 0.75, 0.8, 0.85, 0.9, 0.95, 1}. Second, $\Delta G^{\text{water}}_{\text{elec}}$ is calculated by fixing $\lambda_{\text{vdW}} = 1$ and by performing one Monte Carlo simulation per value of λ_C . The following 11 values of λ_C are selected: {0, 0.1, 0.2, 0.3, 0.4, 0.5, 0.6, 0.7, 0.8, 0.9, 1}. Third, ΔG^{vacuum} is calculated by performing simulations in the same manner as $\Delta G^{\text{water}}_{\text{vdW}}$, but Monte Carlo simulation parameters differ as explained below.

Except for the calculation of ΔG^{vacuum} , a Monte Carlo simulation consists in simulating a NPT ensemble at 298.15 K and 0.1 MPa, with one molecule of solute, and a total of 300 molecules of water. Water is modeled with the TIP4P/2005 force field.⁴⁹ A simulation run lasted for 90 million steps,

including an equilibrium run of 40 million steps. The different Monte Carlo moves and their corresponding attempt probabilities used during the simulations are molecular translation (30%), molecular rotation (30%), regrowth with configurational bias³⁴ (39.5%), and volume change (0.5%). Other simulation parameters are identical to those previously described for phase equilibrium calculation. For the calculation of ΔG^{vacuum} , a Monte Carlo simulation consists in simulating a NPT ensemble at 298.15 K and 0.1 MPa containing only one solute molecule. A simulation run lasted for 5 million MC steps including an equilibrium run of 1 million MC steps, and only regrowth moves with configurational bias are carried out.

4. RESULTS

4.1. Pure Compound Phase Equilibrium. All calculated saturated liquid densities, vapor pressures, and vaporization enthalpies for pure acetic acid, propanoic acid, butanoic acid, pentanoic acid, hexanoic acid, and 1,5-pentanedioic acid are given in Table S.1 in the Supporting Information. A plot of these properties versus temperature is given in Figure 2 for acetic acid and hexanoic acid. The same figure for the other acids studied is given in the Supporting Information (Figure S.3). A plot of the deviation between simulations and experiments as a function of the reduced temperature is shown in Figure 3. Note that the term “experiments” means in this context the reference values given by the DIPPR database.³⁰ It can be either real experimental data or smoothed data from experiments at lower temperatures. Figure 3a shows that saturated liquid densities are predicted with a good agreement (deviations generally range between 0 and +2%) up to reduced temperatures of 0.9. Above this point, deviations become larger for short acids (acetic and propanoic) and for the diacid, while deviations for longer monoacids remain less than 2%. Concerning vapor pressure predictions, deviations generally range from −10 to 10%, and the absolute average deviation for each compound is found of the same order of magnitude as those observed for other oxygenated compounds simulated with the AUA4 force field (typically between 5 to 8%). This is a considerable improvement compared to the TraPPE-UA force field for which average deviations of 50% are reported by Clifford et al. for this property. It can be observed that calculated vapor pressures are generally underestimated for short acids, while they are rather overestimated for longer acids and the diacid studied. Finally, Figure 3c shows that predictions of vaporization enthalpies are not in so good agreement with experiments than other properties. Deviations are the largest (>30%) for short acids at low reduced temperatures. When increasing the alkyl-chain length and temperature, deviations decrease but still remain important (typically between 10 and 20%). As illustrated in Figure 2, the experimental evolution of the vaporization enthalpy with temperature is drastically different for short acids and long acids. For long acids, a classical trend is observed, with a monotonic decrease of vaporization enthalpy when temperature increases. For short acids, this classical trend is observed only at high reduced temperatures. At lower temperatures, the vaporization enthalpy exhibits a maximum before decreasing when temperature decreases. This unusual behavior can be attributed to a large number of molecular associations in the vapor phase through hydrogen bond formation (dimerization phenomenon). As described further, our model exhibits such associations in the vapor phase. However, the number of associated molecules is probably too low to reproduce this maximum in the

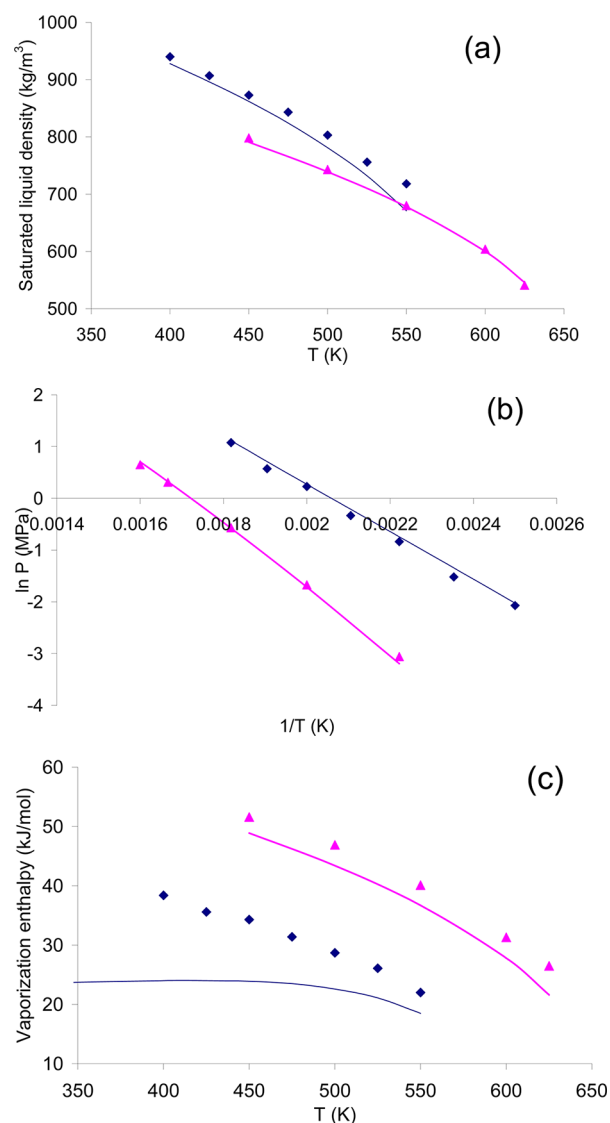


Figure 2. Experimental³⁰ (lines) and calculated (symbols) saturated liquid densities (a), vapor pressures (b), and vaporization enthalpies (c) of acetic acid (blue diamonds and lines) and hexanoic acid (pink triangles and lines).

vaporization enthalpy curve. This point is clearly a limitation of this model. A possible improvement could consist in considering the dimerization phenomenon as a chemical reaction and the dimer as a single molecule, and to simulate the binary system acetic acid (monomer) + acetic acid (dimer) in the reactive Gibbs ensemble.⁵⁰

We also compare our results to predictions obtained with other force fields. For reduced temperatures ranging from 0.68 to 0.93, the average error obtained for saturated liquid densities with the TraPPE-UA force field is 1.6%, with OPLS-UA force field 6.4%, with OPLS-AA force field 1.7% and with the CHARMM force field 14.7% (from values reported by Kamath et al.⁹). For this property, our model is then worse than TraPPE-UA and OPLS-AA, but better than OPLS-UA and CHARMM. However, all these force fields fail to accurately predict vapor pressures (average error with TraPPE-UA: 38%, with OPLS-UA: 76%, with OPLS-AA: 58%, with CHARMM: 179%). Thus, our new model gives a significant improvement to predict this property. During the parameter optimization

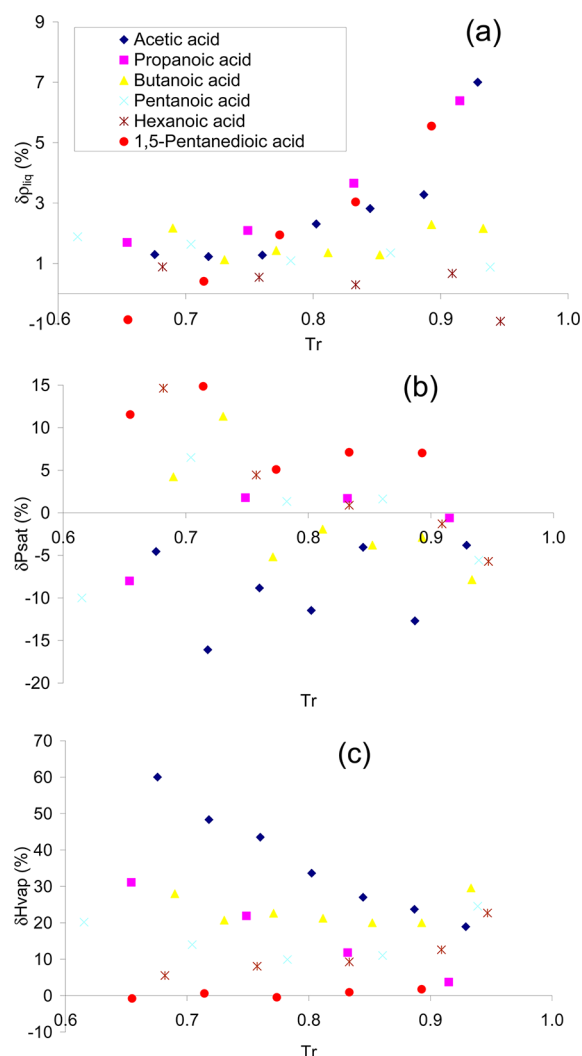


Figure 3. Relative deviations of saturated liquid densities (a), vapor pressures (b), and vaporization enthalpies (c) between simulation data and experimental data ($\delta X = (X_{\text{sim}} - X_{\text{exp}})/X_{\text{exp}} \times 100$).

procedure, the aim was to find the better compromise between a good representation of both saturated liquid densities and vapor pressures. If we consider results up to a reduced temperatures of 0.9, the average deviations obtained are 2% and 9.5%, respectively. Such deviations are of the same order of magnitude as the ones obtained with other oxygenated compounds (alcohols, ethers, etc.) simulated with the AUA4 force field.

According to our experience, Lennard-Jones parameters and partial charges do not affect in the same way the physical properties. Lennard-Jones parameters mainly impact liquid

densities whereas partial charges mainly affect vapor pressures. Thus, to improve liquid density predictions, it can be envisaged to modify the Lennard-Jones parameters of a group (e.g., carboxyl oxygen or hydroxyl group). However, the main objective of this work is to keep the transferability of the AUA4 force field and to reuse existing groups. Thus, this modification is not planned.

Critical properties and normal boiling points calculated with this new model are given in Table 3. The statistical uncertainty in critical temperatures and critical densities are estimated to be ± 4 K and ± 5 kg/m³. These values are consistent with reported values in the literature.^{14,51} Critical densities and normal boiling points are accurately predicted with average deviations of 1.8 and 0.8%, respectively. Critical temperatures of short acids and the diacid are slightly overestimated with deviations from 5 to 7%, but deviations decrease when the alkyl-chain length increases. This behavior is similar to that observed for alcohols with this force field,²⁴ and is thus probably due to the OH group parametrization. An improvement of the critical point prediction could consist in adjusting the scaling exponent β in eq 9 as done by various authors,^{11,52} but the methodology then loses in transferability.

4.2. Liquid and Vapor Phase Structure. The intermolecular radial distribution functions (rdf) of liquid acetic acid have been plotted at 300 K and 0.1 MPa in Figure 4. A comparison with experimental rdf and rdf calculated with other transferable force fields (OPLS-UA,⁸ TraPPE-UA⁹) as reported in the literature is also provided. In this figure, H stands for the hydroxyl hydrogen, O for the hydroxyl oxygen, and OC for the carbonyl oxygen. Except for H–O and OC–OC rdf, an acceptable agreement between our force field predictions and experiments is obtained: the number of peaks, their intensity, and their location are correctly predicted. Both models and experiments exhibit a large peak around 1.8 Å and 2.7 Å for the H–OC and the O–OC rdf, respectively. This configuration is compatible with hydrogen bond formation between the H and the OC atoms. The OC–OC rdf shows an important peak at 3.3 Å for both our new force field and OPLS-UA while experiments give rather a shoulder. This distance can be attributed to the formation of cyclic dimers with two hydrogen bonds per molecule between H and OC atoms, as illustrated in Figure 5a. Thus, it seems that simulations tend to overestimate the number of cyclic dimers in the liquid phase compared to experiments. For the H–O rdf, a small peak is observed at 1.8 Å, while a larger peak is noted at 3.6 Å. The first small peak corresponds to the formation of hydrogen bonds between H and O atoms. Its weak intensity indicates that hydrogen bonds are preferentially formed between H and OC atoms rather than H and O atoms. Our new force field is not in agreement with experiments since this peak is not predicted, which indicates that hydrogen bonds do not appear between these two atoms.

Table 3. Experimental³⁰ and Calculated Critical Points and Normal Boiling Points of the Molecules Studied

	T_c (K)			ρ_c (kg/m ³)			T_b (K)		
	sim.	exp.	AAD(%)	sim.	exp.	AAD(%)	sim.	exp.	AAD(%)
acetic acid	624	592	5.4	341	339	0.6	394	391	0.8
propanoic acid	633	601	5.3	321	315	1.9	421	414	1.7
butanoic acid	638	616	3.6	301	301	0.0	434	436	0.5
pentanoic acid	656	639	2.7	289	292	1.0	462	459	0.7
hexanoic acid	675	660	2.3	282	285	1.1	476	479	0.8
1,5-pentanedioic acid	897	840	6.8	369	347	6.3	598	600	0.3

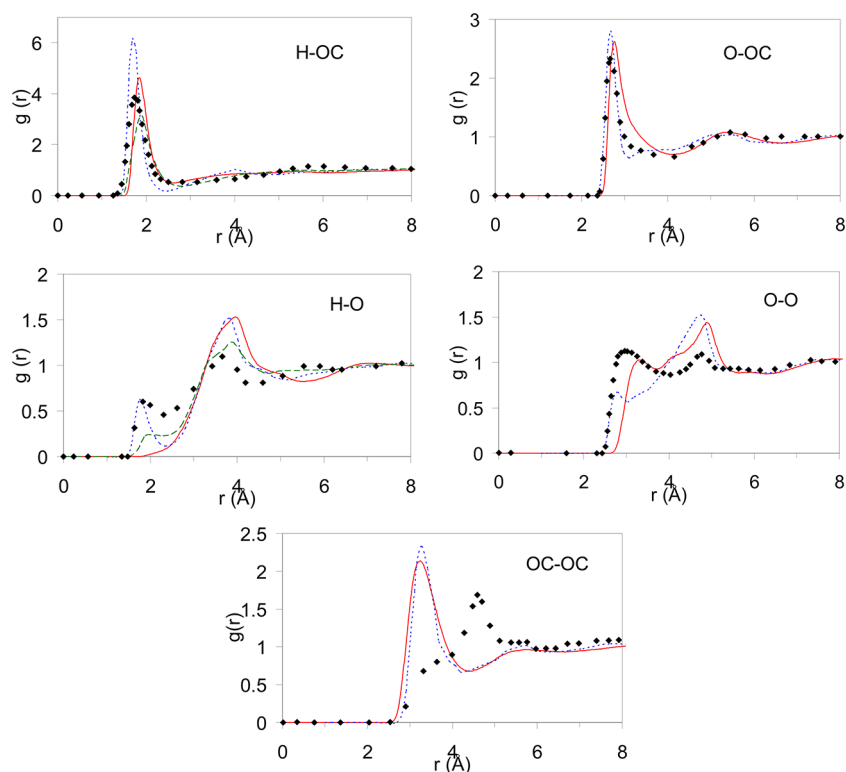


Figure 4. Radial distribution functions in liquid acetic acid at 300 K, 0.1 MPa. Symbols: experiments;⁶⁰ Solid red line: this work; dashed blue line: OPLS-UA force field;⁸ dashed-dotted green line: TraPPE-UA force field.^{9,11}

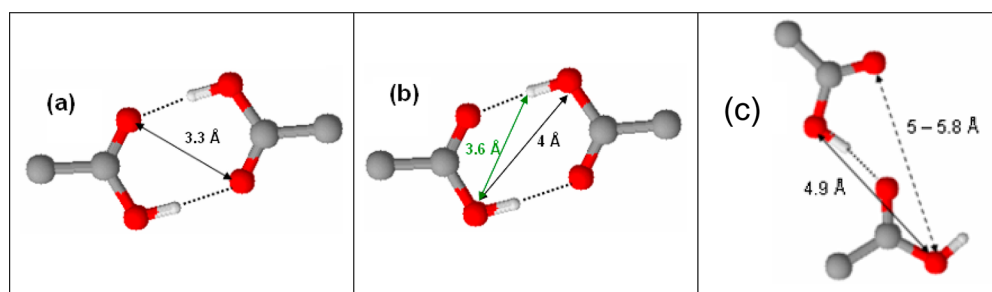


Figure 5. (a,b) Scheme of a cyclic acetic acid dimer with two hydrogen bonds per molecule with the characteristic distance OC–OC (a), H–O (b), and O–O (b). (c) Scheme of a noncyclic acetic acid dimer with the characteristic distance O–O and O–OC.

It can be noticed that the OPLS-UA force field correctly predicts this peak, whereas the TraPPE-UA force field tends to predict rather a shoulder. In this rdf, the second large peak at 3.6 Å (shifted at 4 Å with our new force field) is compatible with the formation of cyclic dimers as previously mentioned and illustrated in Figure 5b. For the O–O rdf, a shoulder at 4 Å is predicted with our force field, compatible with the cyclic dimer structure illustrated in Figure 5b. A peak at 2.8 Å corresponding to the hydrogen bond formation between O and H is observed both in experiments and in the OPLS-UA force field, but not with this model. This is consistent with the previous analysis of the H–O rdf. As discussed by Briggs et al., the second peak at 4.9 Å observed experimentally and well predicted with the force fields can be attributed to a noncyclic dimerization of acetic acid illustrated in Figure 5c. This structure is compatible with the second peak of the O–OC rdf observed around 5–5.8 Å with both experiments and models. Finally, the distribution of hydrogen bond number per acetic acid molecule is given in Table 4 and compared to results obtained with the OPLS-UA force field as reported by Briggs et

Table 4. Distribution of the Number of Hydrogen Bonds Per Molecule (n) in Liquid Acetic Acid at 300 K, 0.1 MPa

n	this work	OPLS-UA force field ⁸
0	0.3	1.3
1	33.3	25.4
2	40.8	64.1
3	19.4	8.8
4	5.4	0.3
5	0.8	0.0

al.⁸ A hydrogen bond is defined here by a oxygen–oxygen distance ranging from 2.5 to 4.1 Å (first minima of the OC–O rdf) and O–H...O angle ranging from 90 to 180°. Note that this definition slightly differs from that used by Briggs et al., who define the hydrogen bond by a O–H distance less than 2.41 Å and an interaction energy less than −4.0 kcal/mol. Both models give similar results, with a maximum of the distribution for a number of 2 hydrogen bonds per molecule, compatible with simple cyclic dimers as illustrated in Figure 5a. Note that if

we consider that a dimerization occurs when at least one hydrogen bond per molecule exists, both models are also in good agreement with a predicted monomer fraction of 0.3% (this model) versus 1.3% (OPLS-UA force field).

The structure of acetic acid in a vapor phase at 425 K and 0.219 MPa (vapor pressure) is also studied, and rdf's are given in Figure S.4. in the Supporting Information. The H–OC and O–OC rdf's clearly exhibit a large peak around 2 and 3 Å, respectively, indicating the formation of hydrogen bonds between these two atoms. Using the geometric criteria previously given to define the hydrogen bond, a monomer fraction equal to 0.73 is found in the vapor phase, which means that 27% of the acetic acid molecules are hydrogen bonded. This value is probably underpredicted since no significant impact on vaporization enthalpy is observed. The distribution of hydrogen bond number per acetic acid molecule in the vapor phase is given in Table S.2 in the Supporting Information.

4.3. Binary Mixtures. To evaluate the transferability of the new force field to mixtures, two binary systems are studied: acetic acid + *n*-butane at 323.15 K, and propanoic acid + pentanoic acid at 393.15 K. The *n*-butane is modeled with the AUA4 force field for hydrocarbons.¹² Results are plotted in Figures 6 and 7 as well as experimental data.^{53,54} Both mixtures

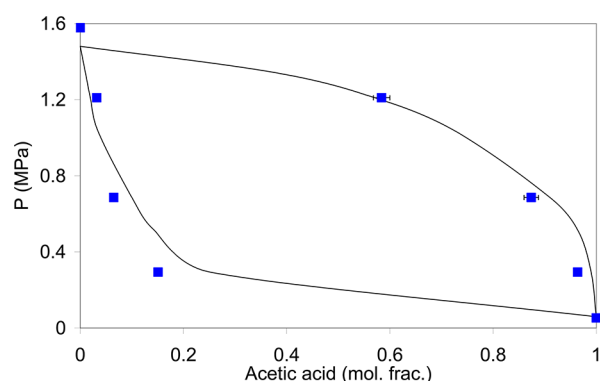


Figure 6. Pressure–composition diagram of the acetic acid + *n*-butane binary mixture at 373.15 K. Solid line: smoothed experimental data;⁵³ filled symbols: this work.

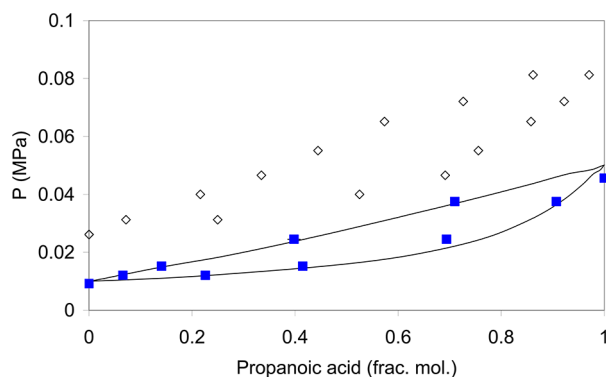


Figure 7. Pressure–composition diagram of the propanoic acid + pentanoic acid binary mixture at 393.15 K. Solid line: smoothed experimental data;⁵⁴ filled symbols: this work; open symbols: TraPPE-UA force field.¹¹

are accurately predicted with the new force field. It is worth noticing that no empirical binary interaction parameters are required to obtain such accuracy, thus highlighting the transferability of the new force field to mixtures. A significant

improvement is brought compared to results obtained with the TraPPE-UA force field with which bubble and dew pressures are strongly overestimated.¹¹

4.4. Hydration Free Energy. Figure 8 shows the variation of $\langle dU/d\lambda \rangle$ versus λ for both van der Waals and electrostatic

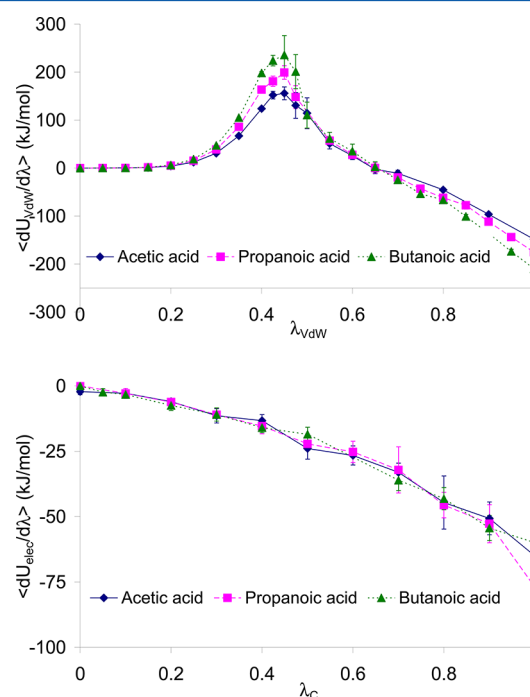


Figure 8. Average derivatives of the van der Waals and electrostatic energies with respect to λ_{vdW} and λ_C .

energy for the three acids studied (acetic acid, propanoic acid, and butanoic acid). For the van der Waals contribution, the curve exhibits a maximum: as discussed by Wan et al.,⁵⁵ this specific shape can be attributed to two counterbalancing factors: unfavorable excluded volume effects due to cavity creation in the solvent, and favorable solute–solvent interactions. These van der Waals and electrostatic curves are integrated between 0 and 1 to obtain free energy given by eq 12 using the trapezoid method. Table 5 reports the “insertion” contribution ΔG_{vdW}^{water} , the “charging” contribution ΔG_{elec}^{water} and the intramolecular contribution ΔG^{vacuum} of the free energy, as defined in eq 11, as well as the total hydration free energy ΔG^{hyd} . In this table are also reported experimental data⁵⁶ and calculations using the TraPPE-UA force field in the case of

Table 5. Hydration Free Energy Calculated with This New Force Field, the TraPPE-UA Force Field,⁵⁷ and Experimental Data^{56a}

solute	source	ΔG_{vdW}^{water} (kJ/mol)	ΔG_{elec}^{water} (kJ/mol)	ΔG^{vacuum} (kJ/mol)	ΔG^{hyd} (kJ/mol)
acetic acid	this work	7.0 ₃	−24.6 ₄	0	−17.6 ₅
	exp.	−	−	−	−28.0
	TraPPE-UA	3.54 ₁₁	−21.31 ₃	0	−17.77 ₁₁
propanoic acid	this work	8.1 ₂	−25.1 ₆	0	−17.1 ₆
	exp.	−	−	−	−27.1
butanoic acid	this work	9.0 ₃	−24.8 ₅	−0.3 ₀	−15.5 ₅
	Exp.	−	−	−	−26.6

^aThe subscript on calculated data gives the statistical uncertainty on the last digit (for example, 7.0₃ means 7 ± 0.3).

acetic acid as reported by Garrido et al.⁵⁷ The behavior of the hydration free energy is qualitatively well predicted since this energy increases with the length of the alkyl chain as observed experimentally. This can be attributed to an increase of the hydrophobic part of the molecule when the alkyl chain increases. However, from a quantitative point of view, the calculated free hydration energy are significantly overestimated compared to experimental values (deviations about 10 kJ/mol). The relative hydration free energy between two acids is, however, well predicted: the addition of one methylene group in the alkyl chain leads to an increase of around 1 kJ/mol, which is the order of magnitude observed experimentally. It can also be emphasized that the use of the TraPPE-UA force field provided similar results and deviations for acetic acid.⁵⁷ Using a united-atoms force field parametrized only on phase equilibrium properties seems to be inadequate to predict with a good accuracy the absolute hydration free energy of acids, but only relative hydration free energies. Thus, the use of all-atoms force fields appears necessary to obtain quantitative results for this property, probably due to a better description of the liquid phase structure or a better account of solute–solvent interactions. The choice of the model for water could also be questionable. Many models are actually available (SPC, SPC/E, TIP4P, TIP4P/2005, etc.) with each of them advantages and drawbacks. To compute hydration free energy of polar compounds with the TraPPE-UA force field, Garrido et al.⁵⁷ used the MSPC/E force field for water.⁵⁸ A good accuracy was obtained for some molecule families (alcohols, amines), but similar high deviations were observed for acetic acid. Thus, it seems that the source of error should be preferentially attributed to the force field of acids and not to that of water. Furthermore, a probable improvement could consist in a better consideration of polarization effects in the force field. It is well-known that polarization leads to a lowering of hydration free energy.⁵⁹ In this new force field, the partial electrostatic charges reproduce the gas phase dipole moment, and the polarization effect on the solute due to the electric field of water is probably not correctly taken into account.

5. CONCLUSION

In this work, a new transferable united-atom force field has been developed to predict phase equilibrium and hydration free energy of carboxylic acids. To take advantage of the transferability of the AUA4 force field, all Lennard-Jones parameters of groups involved in the carboxylic acid chemical function are reused from previous parametrizations of this force field. Only a unique set of partial electrostatic charges is proposed to reproduce the experimental gas phase dipole moment, saturated liquid densities and vapor pressures. Phase equilibrium properties of various pure carboxylic acids (acetic acid, propanoic acid, butanoic acid, pentanoic acid, hexanoic acid) and one diacid (1,5-pentanedioic) are studied through Monte Carlo simulations in the Gibbs ensemble. A good accuracy is obtained for pure compound saturated liquid densities and vapor pressures (average deviation of 2% and 6%, respectively), as well as for critical points. The vaporization enthalpy is, however, poorly predicted for short acids, probably due to a limitation of the force field to correctly describe the significant dimerization in the vapor phase. Pressure–composition diagrams for two binary mixtures (acetic acid + *n*-butane and propanoic acid + pentanoic acid) are also computed with a good accuracy, showing the transferability of the proposed force field to mixtures. Hydration free energies

are calculated for three carboxylic acids using thermodynamic integration. A systematic overestimation of around 10 kJ/mol is observed compared to experimental data. This new force field parametrized only on phase equilibrium properties appears insufficient to reach an acceptable precision for this property, and only relative hydration free energies between two carboxylic acids can be correctly predicted. This highlights the limitation of the transferability feature of force fields to properties not included in the parametrization database.

■ ASSOCIATED CONTENT

Supporting Information

Numerical values of simulation results (Table S.1), hydrogen bonds number distribution in vapor phase (Table S.2), scheme of Lennard-Jones parameters reused (Figure S.1), experimental gas phase dipole moment (Figure S.2.), additional simulation results (Figure S.3), and vapor phase rdf (Figure S.4). This material is available free of charge via the Internet at <http://pubs.acs.org>.

■ AUTHOR INFORMATION

Corresponding Author

*Tel: +33 147526624. Fax: +33 147527025. E-mail: nicolas.ferrando@ifpen.fr.

Notes

The authors declare no competing financial interest.

■ ACKNOWLEDGMENTS

We gratefully acknowledge the ANR for support of this work through Grant ANR-09-CP2D-10-04 MEMOBIOL. This work was granted access to the HPC resources of CCRT/CINES under the allocation 2011-X2011096349 and 2012-X2012096349 made by GENCI (Grand Equipement National de Calcul Intensif).

■ REFERENCES

- (1) Huber, G. W.; Iborra, S.; Corman, A. *Chem. Rev.* **2006**, *106*, 4044–4098.
- (2) Huber, G. W.; Corma, A. *Angew. Chem., Int. Ed.* **2007**, *46*, 7184–7201.
- (3) Lin, L.; Zhou, C. S.; Vittayapadung, S.; Shen, X. Q.; Dong, M. D. *Appl. Energy* **2011**, *88*, 1020–1031.
- (4) Atadashi, I. M.; Aroua, M. K.; Aziz, A. A. *Renewable Energy* **2011**, *36*, 437–443.
- (5) Theodorou, D. N. *Ind. Eng. Chem. Res.* **2010**, *49*, 3047–3058.
- (6) Ungerer, P.; Nieto-Draghi, C.; Lachet, V.; Wender, A.; Di Lella, A.; Boutin, A.; Rousseau, B.; Fuchs, A. H. *Mol. Sim.* **2007**, *33*, 287–304.
- (7) Ungerer, P.; Tavittian, B.; Boutin, A. *Applications of Molecular Simulation in the Oil and Gas Industry*, 1st ed.; Editions Technip: Paris, 2005.
- (8) Briggs, J. M.; Nguyen, T. B.; Jorgensen, W. L. *J. Phys. Chem.* **1991**, *95*, 3315–3322.
- (9) Kamath, G.; Cao, F.; Potoff, J. J. *J. Phys. Chem. B* **2004**, *108*, 14130–14136.
- (10) Martin, M. G.; Siepmann, J. I. *J. Phys. Chem. B* **1998**, *102*, 2569–2577.
- (11) Clifford, S.; Bolton, K.; Ramjugernath, D. *J. Phys. Chem. B* **2006**, *110*, 21938–21943.
- (12) Ungerer, P.; Beauvais, C.; Delhommelle, J.; Boutin, A.; Rousseau, B.; Fuchs, A. H. *J. Chem. Phys.* **2000**, *112*, 5499–5510.
- (13) Bourasseau, E.; Ungerer, P.; Boutin, A.; Fuchs, A. H. *Mol. Simul.* **2002**, *28*, 317–336.
- (14) Bourasseau, E.; Ungerer, P.; Boutin, A. *J. Phys. Chem. B* **2002**, *106*, 5483–5491.

- (15) Bourasseau, E.; Haboudou, M.; Boutin, A.; Fuchs, A. H.; Ungerer, P. *J. Chem. Phys.* **2003**, *118*, 3020–3034.
- (16) Contreras-Camacho, R. O.; Ungerer, P.; Boutin, A.; Mackie, A. D. *J. Phys. Chem. B* **2004**, *108*, 14109–14114.
- (17) Bonnaud, P.; Nieto-Draghi, C.; Ungerer, P. *J. Phys. Chem. B* **2007**, *111*, 3730–3741.
- (18) Contreras-Camacho, R. O.; Ungerer, P.; Ahunbay, M. G.; Lachet, V.; Perez-Pellitero, J.; Mackie, A. D. *J. Phys. Chem. B* **2004**, *108*, 14115–14123.
- (19) Nieto-Draghi, C.; Bonnaud, P.; Ungerer, P. *J. Phys. Chem. C* **2007**, *111*, 15686–15699.
- (20) Ahunbay, M. G.; Perez-Pellitero, J.; Contreras-Camacho, R. O.; Teuler, J. M.; Ungerer, P.; Mackie, A. D.; Lachet, V. *J. Phys. Chem. B* **2005**, *109*, 2970–2976.
- (21) Creton, B.; de Bruin, T.; Lachet, V.; Nieto-Draghi, C. *J. Phys. Chem. B* **2010**, *114*, 6522–6530.
- (22) Delhommelle, J.; Tschirwitz, C.; Ungerer, P.; Granucci, G.; Millie, P.; Pattou, D.; Fuchs, A. H. *J. Phys. Chem. B* **2000**, *104*, 4745–4753.
- (23) Perez-Pellitero, J.; Ungerer, P.; Mackie, A. D. *J. Phys. Chem. B* **2007**, *111*, 4460–4466.
- (24) Ferrando, N.; Lachet, V.; Teuler, J. M.; Boutin, A. *J. Phys. Chem. B* **2009**, *113*, 5985–5995.
- (25) Ferrando, N.; Lachet, V.; Boutin, A. *J. Phys. Chem. B* **2010**, *114*, 8680–8688.
- (26) Ferrando, N.; Lachet, V.; Perez-Pellitero, J.; Mackie, A. D.; Malfreyt, P.; Boutin, A. *J. Phys. Chem. B* **2011**, *115*, 10654–10664.
- (27) Ferrando, N.; Lachet, V.; Boutin, A. *J. Phys. Chem. B* **2012**, *116*, 3239–3248.
- (28) Orozco, G. A.; Nieto-Draghi, C.; Mackie, A. D.; Lachet, V. *J. Phys. Chem. B* **2011**, *115*, 14617–14625.
- (29) Orozco, G. A.; Nieto-Draghi, C.; Mackie, A. D.; Lachet, V. *J. Phys. Chem. B* **2012**, *116*, 6193–6202.
- (30) Rowley, R. L.; Wilding, W. V.; Oscarson, J. L.; Yang, Y.; Zundel, N. A.; Daubert, T. E.; Danner, R. P. *DIPPR® Data Compilation of Pure Compounds Properties*; Design Institute for Physical Properties, AIChE: New York, 2003.
- (31) Panagiotopoulos, A. Z. *Mol. Phys.* **1987**, *61*, 813–826.
- (32) Panagiotopoulos, A. Z. *Mol. Simul.* **1992**, *9*, 1–23.
- (33) Allen, M. P.; Tildesley, D. J. *Computer Simulation of Liquids*; Oxford University Press: New York, 1987.
- (34) Frenkel, D.; Smit, B. *Understanding Molecular Simulation: From Algorithms to Applications*; Academic Press: San Diego, CA, 1996.
- (35) Mackie, A. D.; Tavittian, B.; Boutin, A.; Fuchs, A. H. *Mol. Simul.* **1997**, *19*, 1–15.
- (36) Panagiotopoulos, A. Z.; Quirke, N.; Stapleton, M.; Tildesley, D. *J. Mol. Phys.* **1988**, *63*, 527–545.
- (37) Zwanzig, R. W. *J. Chem. Phys.* **1954**, *22*, 1420–1426.
- (38) Nezbeda, I.; Kolafa, J. *Mol. Simul.* **1991**, *5*, 391–403.
- (39) Torrie, G. M.; Valleau, J. P. *J. Comput. Phys.* **1977**, *23*, 187–199.
- (40) Chipot, C.; Pohorille, A. *Free Energy Calculations*; Springer Series in Chemical Physics; Springer: Berlin/Heidelberg/New York, 2007.
- (41) Leach, A. *Molecular Modeling: Principles and Applications*; Prentice-Hall: Harlow, 2001.
- (42) Economou, I. G.; Garrido, N. M.; Makrodimitri, Z. A. *Fluid Phase Equilib.* **2010**, *296*, 125–132.
- (43) Garrido, N. M.; Queimada, A. J.; Jorge, M.; Macedo, E. A.; Economou, I. G. *J. Chem. Theory Comput.* **2009**, *5*, 2436–2446.
- (44) Shirts, M. R.; Pitner, J. W.; Swope, W. C.; Pande, V. S. *J. Chem. Phys.* **2003**, *119*, 5740–5761.
- (45) Beutler, T. C.; Mark, A. E.; Vanschaik, R. C.; Gerber, P. R.; Vangunsteren, W. F. *Chem. Phys. Lett.* **1994**, *222*, 529–539.
- (46) Garrido, N. M.; Jorge, M.; Queimada, A. J.; Economou, I. G.; Macedo, E. A. *Fluid Phase Equilib.* **2010**, *289*, 148–155.
- (47) Chang, J. *J. Chem. Phys.* **2009**, *131*, 074103.
- (48) Partay, L.; Jedlovsky, P.; Jancso, G. *J. Phys. Chem. B* **2005**, *109*, 8097–8102.
- (49) Abascal, J. L. F.; Vega, C. *J. Chem. Phys.* **2005**, *123*, 234505.
- (50) Smith, W. R.; Triska, B. *J. Chem. Phys.* **1994**, *100*, 3019–3027.
- (51) Harris, J. G.; Yung, K. H. *J. Phys. Chem.* **1995**, *99*, 12021–12024.
- (52) Chen, B.; Potoff, J. J.; Siepmann, J. I. *J. Phys. Chem. B* **2001**, *105*, 3093–3104.
- (53) Krichevskii, I. R.; Efremova, G. D.; Pryanikova, R. O.; Polyakov, E. E. *Khim. Prom-st. (Moscow)* **1961**, *7*, 498–502.
- (54) Clifford, S. L.; Ramjugernath, D.; Raal, J. D. *Fluid Phase Equilib.* **2005**, *237*, 89–99.
- (55) Wan, S.; Stote, R. H.; Karplus, M. *J. Chem. Phys.* **2004**, *121*, 9539–9548.
- (56) Hine, J. *J. Org. Chem.* **1975**, *40*, 292–298.
- (57) Garrido, N. M.; Queimada, A. J.; Jorge, M.; Economou, I. G.; Macedo, E. A. *Fluid Phase Equilib.* **2010**, *296*, 110–115.
- (58) Boulougouris, G. C.; Economou, I. G.; Theodorou, D. N. *J. Phys. Chem. B* **1998**, *102*, 1029–1035.
- (59) Hess, B.; van der Vegt, N. F. A. *J. Phys. Chem. B* **2006**, *110*, 17616–17626.
- (60) Imberti, S.; Bowron, D. T. *J. Phys.: Condens. Matter* **2010**, *22*, 404212.